Optics Letters

Giant thermo-optical relaxation oscillations in millimeter-size whispering gallery mode disk resonators

SOULEYMANE DIALLO, GUOPING LIN, AND YANNE K. CHEMBO*

FEMTO-ST Institute, CNRS—Université Bourgogne Franche-Comté, Optics Department, 15B Avenue des Montboucons, 25030 Besançon cedex, France
**Corresponding author: yanne.chembo@femto-st.fr*

Received 12 May 2015; revised 16 July 2015; accepted 21 July 2015; posted 21 July 2015 (Doc. ID 240828); published 10 August 2015

In this Letter, we show that giant thermo-optical oscillations can be triggered in millimeter (mm)-size whispering gallery mode (WGM) disk resonators when they are pumped by a resonant continuous-wave laser. Our resonator is an ultrahigh-Q barium fluoride cavity that features a positive thermo-optic coefficient and a negative thermo-elastic coefficient. We demonstrate for the first time, to our knowledge, that the complex interplay between these two thermic coefficients and the intrinsic Kerr nonlinearity yields very sharp slow–fast relaxation oscillations with a slow timescale that can be exceptionally large, typically of the order of 1 s. We use a time-domain model to gain understanding into this instability, and we find that both the experimental and theoretical results are in excellent agreement. The understanding of these thermal effects is an essential requirement for every WGM-related application and our study demonstrates that even in the case of mm-size resonators, such effects can still be accurately analyzed using nonlinear time-domain models.

OCIS codes: (190.4870) Photothermal effects; (160.6840) Thermo-optical materials; (230.4910) Oscillators; (160.4330) Nonlinear optical materials.

http://dx.doi.org/10.1364/OL.40.003834

Optical whispering gallery mode (WGM) resonators are monolithic cavities that can feature ultrahigh quality factors (up to $\sim 10^{11}$ at 1 μm) and small mode volume. They can be used in several applications such as laser stabilization [1–5], sensing [6–8], or optical frequency comb generation (see Ref. [9] and references therein).

When these resonators are pumped with a resonant continuous-wave (CW) laser, the pump photons are trapped by total internal reflection within the torus-like modes of the resonator for time durations that can be as long as few microseconds. As a consequence, the laser field is significantly enhanced in the mode volume, and strongly heats the disk resonator close to its inner periphery. From an intuitive viewpoint, one may consider that the heat originating from this local increase in temperature would smoothly diffuse both inside and outside the bulk resonator, and asymptotically lead to a space-dependent, but time-independent (stationary), distribution of temperature. This is actually always the case when the pump power is sufficiently low, regardless of the thermal properties of the resonator.

However, when the power of the pump laser is high enough, the dynamics of the temperature in the mode volume and in the bulk cavity can become time dependent, and display very complex relaxation oscillations. Such a counterintuitive behavior has already been evidenced and analyzed in microspheres, where the very small mode and resonator volumes are likely to be strongly affected by temperature increase through thermal expansion [10–14]. Indeed, the effect of temperature is to induce a resonance shift for the WGMs, which affects the input energy rate (since the laser frequency is fixed), and ultimately, the temperature of the resonator. This feedback loop might be unstable depending on the parameters of the system, and it was shown that nonlinear time-domain models could be used to gain understanding of this complex phenomenology. Nevertheless, such relaxation oscillations have never been observed in millimeter (mm)-size WGM resonators, where the resonator volume is significantly larger than the mode volume. Most of the time, mm-size WGM resonators are operated in the regime of so-called *thermal locking*, where temperature-induced resonance shifts play a beneficial role with regards to the stabilization of the pumped resonator.

In this Letter, we present the first experimental observation, to our knowledge, of relaxation oscillations in a ultrahigh-Q mm-size WGM resonators. The bulk material of our monolithic cavity is barium fluoride (BaF_2), and we demonstrate that the interplay between thermal and nonlinearity-induced shifts can lead to sharp relaxation oscillations whose period is of the order of 1 s. We also present a theoretical model that is able to match experimental results with excellent accuracy.

The experimental setup is shown in Fig. 1. A tunable CW fiber laser with subkilohertz instantaneous linewidth at 1550 nm was used to pump the ultrahigh-Q barium fluoride disk resonator. Optical WGMs were excited using a SF11 prism

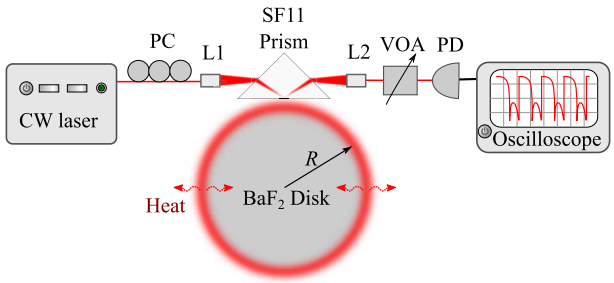

Fig. 1. Schematic illustration of the experimental setup. PC, fiber polarization controller; VOA, variable optical attenuator; L1, L2, GRIN lenses; PD, photodetector.

as the evanescent wave coupler. The first pigtailed gradient-index (GRIN) lens focuses the incident light on the prism for the WGM coupling, while the second lens collects the reflected light for the detection by a photodiode with a digital oscilloscope. A piezoelectric actuator was used to accurately control the coupling gap between the prism and the resonator.

As illustrated in Fig. 2, when pumped with laser light, the mode volume hosting the intracavity field is subjected to a strong increase of temperature, and subsequently, this modal volume plays the role of a hot source, which diffuses the heat inside the bulk resonator. The resonator transfers part of this heat to the surroundings. This thermal dynamics induces a resonance shift through two distinct mechanisms. The first one is that the refraction index is temperature dependent, and therefore, the bulk optical properties, such as the group velocity, are affected by the intracavity field via the induced heat transfer. This effect is essentially restricted to the modal volume. The second reason is that as the bulk resonator heats up, it undergoes a thermal dilatation that modifies its main radius. Both effects induce a shift of the free-spectral range, or equivalently, of the WGM resonances. The overall frequency shift caused by thermal effects can be explicitly expressed as

$$\Delta\omega_{\mathrm{th}}(t) = -\omega_{\mathrm{c}}[\alpha_1 \Delta T_1(t) + \alpha_2 \Delta T_2(t)], \tag{1}$$

where ω_{c} is the angular frequency of resonance, ΔT_1 is the shift temperature of the modal volume, ΔT_2 is the average temperature shift of the full resonator, and the parameters $\alpha_{1,2}$ are the coefficients that enable the conversion from temperature to frequency shift. The two effects highlighted above can be of stochastic or deterministic nature, depending on if the variables ΔT_1 and ΔT_2 correspond to fast-timescale thermodynamic fluctuations or to slow-timescale thermal shifts. In the stochastic case, these thermal effects are associated to fundamental fluctuations set by the laws of statistical thermodynamics, while in the deterministic case, thermal effects can induce either a desired locking between the laser and the resonance frequencies, or thermo-optical oscillations [6,12].

The Kerr nonlinearity also induces a local modification of the refraction index, which leads to the resonance shift

$$\Delta\omega_{\mathrm{nl}}(t) = -\omega_{\mathrm{c}}\left[\frac{n_2}{n_{\mathrm{eff}}}\frac{P_{\mathrm{c}}(t)}{A_{\mathrm{eff}}}\right], \tag{2}$$

where n_{eff} is the effective refractive index, n_2 is the Kerr coefficient of the WGM resonator, $P_{\mathrm{c}}(t)$ is the intracavity power, and A_{eff} is the effective cross-sectional area of the WGM resonator. According to formula (4) of Ref. [15], the effective area of a disk resonator with diameter D is of the order of $A_{\mathrm{eff}} \sim D^{\frac{5}{6}}\lambda^{\frac{7}{6}}$, where λ is the laser pump wavelength in the bulk medium. The intracavity power $P_{\mathrm{c}}(t)$ can be expressed as a function of the intracavity field $E_{\mathrm{c}}(t)$ as $P_{\mathrm{c}}(t) = |E_{\mathrm{c}}(t)|^2/T_{\mathrm{r}}$, where $T_{\mathrm{r}} = \pi D n_{\mathrm{eff}}/c$ is the intracavity round-trip time and c is the velocity of light in vacuum.

The dynamics of the intracavity field therefore obeys

$$\frac{dE_{\mathrm{c}}}{dt} = -\left[\frac{1}{2}\delta\omega_Q + i(\sigma + \Delta\omega_{\mathrm{th}} + \Delta\omega_{\mathrm{nl}})\right]E_{\mathrm{c}} + i\frac{k}{T_{\mathrm{r}}}E_{\mathrm{in}}, \tag{3}$$

where $\sigma = \omega_{\mathrm{c}} - \omega_{\mathrm{p}}$ is the cold cavity detuning between the laser pump frequency ω_{p} and the resonance frequency ω_{c}. The parameter $E_{\mathrm{in}} = \sqrt{P_{\mathrm{in}} \times T_{\mathrm{r}}}$ is the amplitude of the input optical field, and $k = \sqrt{T_{\mathrm{r}} \times \Delta\omega_{\mathrm{ext}}}$ is the optical coupling coefficient. The loaded linewidth $\delta\omega_Q = \omega_{\mathrm{c}}/Q$ is the sum of the intrinsic linewidth $\delta\omega_{\mathrm{in}} = \omega_{\mathrm{c}}/Q_{\mathrm{in}}$ and extrinsic (or coupling) linewidth $\delta\omega_{\mathrm{ext}} = \omega_{\mathrm{c}}/Q_{\mathrm{ext}}$, where $Q^{-1} = Q_{\mathrm{in}}^{-1} + Q_{\mathrm{ext}}^{-1}$. The output field of the prism resonator is defined by

$$E_{\mathrm{out}}(t) = \sqrt{1 - k^2}E_{\mathrm{in}} + ikE_{\mathrm{c}}(t), \tag{4}$$

and the normalized transmission explicitly reads

$$\mathcal{T} = \frac{|E_{\mathrm{out}}|^2}{|E_{\mathrm{in}}|^2}, \tag{5}$$

with $0 \le \mathcal{T} \le 1$. This transmission factor will be the dynamical variable of interest for both the experimental and theoretical analysis.

The understanding of the system's behavior also requires a time-domain description of the temperature dynamics. Two different temperature variables have to be accounted for, namely, the temperature of the mode volume and the bulk resonator with respect to the external thermal bath (temperature of the environment). These two variables are respectively labeled as ΔT_1 and ΔT_2, and they obey the equations

$$\frac{d\Delta T_i}{dt} = -\gamma_{\mathrm{th},i}\Delta T_i(t) + \gamma_{\mathrm{abs},i}P_{\mathrm{c}}(t) \quad \text{with} \quad i = 1, 2, \tag{6}$$

where $\gamma_{\mathrm{th},i}$ is effective thermal relaxation rate to ambient temperature, while $\gamma_{\mathrm{abs},i}$ is the effective thermal absorption rate, which weights the heat transfer from to the confined laser field to the mode and resonator volumes.

It is convenient to normalize Eqs. (3) and (6) as

$$\frac{d\xi}{d\tau} = -[1 + i(\varsigma + \beta_1\Delta\theta_1 + \beta_2\Delta\theta_2 + \eta|\xi|^2)]\xi + i\mu, \tag{7}$$

$$\frac{d\Delta\theta_i}{d\tau} = -\rho_i\Delta\theta_i + \kappa_i|\xi|^2, \tag{8}$$

where the dimensionless time τ, intracavity field $\xi(t)$, and relative temperatures $\Delta\theta_i$ are explicitly defined as

$$\tau = \frac{t}{2\tau_{\mathrm{ph}}} \quad \text{with} \quad \tau_{\mathrm{ph}} = \frac{1}{\delta\omega_Q}, \tag{9}$$

$$\xi = \frac{E_{\mathrm{c}}}{E_{\mathrm{ref}}} \quad \text{with} \quad E_{\mathrm{ref}} = \sqrt{\frac{T_r\delta\omega_Q^3}{8\gamma v_g\delta\omega_{\mathrm{ext}}}}, \tag{10}$$

$$\Delta\theta_i = \sqrt{-\alpha_1\alpha_2}\Delta T_i, \tag{11}$$

with τ_{ph} being the photon lifetime in the coupled resonator, $v_g = c/n_{\mathrm{eff}}$ being the group velocity in the bulk resonator,

and $\gamma = \omega_c n_2 / c A_{\text{eff}}$ being the Kerr parameter, which is commonly used in nonlinear guided structures. Note that the reference electric field E_{ref} used for the normalization corresponds to the absolute minimum threshold for Kerr comb generation. The dimensionless parameters of Eqs. (7) and (8) are explicitly defined as

$$\varsigma = \frac{2\sigma}{\delta\omega_Q}, \quad \eta = \frac{-2\omega_c n_2 E_{\text{ref}}^2}{\delta\omega_Q A_{\text{eff}} n_{\text{eff}} T_{\text{r}}}, \quad \mu = \frac{2kE_{\text{in}}}{E_{\text{ref}}\delta\omega_Q T_{\text{r}}}, \tag{12}$$

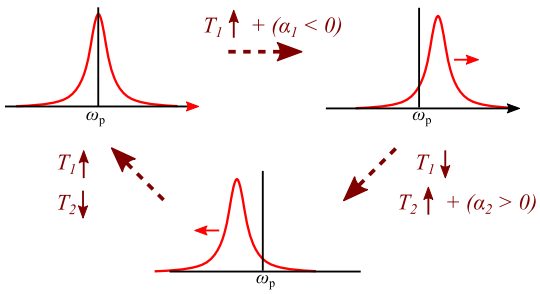

Fig. 2. Scheme of the thermal oscillations. In the first step (top left), the laser is resonant with the cavity. The mode is heated and its temperature increases ($T_1\uparrow$). As a result of this increase of the mode temperature, the resonance is blueshifted because $\alpha_1 < 0$. In the second step (top right), the laser pump becomes off-resonant, thereby leading to a cooling of the mode ($T_1\downarrow$). The heat of the mode diffuses to the bulk resonator ($T_2\uparrow$); the consequent thermal expansion leads to a resonance redshift (induced by $\alpha_2 > 0$). In the third step (bottom), both the mode and the resonator cool down because the laser is still off-resonance ($T_{1,2}\downarrow$). This cooling down process resets the resonance to its initial position, which is resonant with the laser, and the cycle starts again.

$$\rho_i = \frac{2\gamma_{\text{th},i}}{\delta\omega_Q}, \quad \kappa_i = \frac{2E_{\text{ref}}^2\sqrt{-\alpha_1\alpha_2}}{\delta\omega_Q T_{\text{r}}}\gamma_{\text{abs},i},$$
$$\beta_i = \frac{-2\omega_c\alpha_i}{\delta\omega_Q\sqrt{-\alpha_1\alpha_2}}, \tag{13}$$

with $i = 1, 2$. The physical meaning of these dimensionless parameters is fairly transparent.

At the experimental level, our laser was finely tunable using a high-voltage external drive control signal. A triangular ramp was first applied to widely scan the frequency across several optical modes, in order to locate the ultrahigh-Q ones. A barium fluoride WGM resonator with an intrinsic quality factor of 1.0×10^8 was chosen to study its thermal oscillatory behavior. It is noteworthy that billion quality factors can be obtained as well with this crystal [16]. To observe the thermal oscillations, the laser frequency was tuned into the vicinity of the resonance center frequency and then set to a fixed value. The thermal oscillatory behavior was then observed in the transmitted light through the prism–resonator coupling setup, as shown in Fig. 1. We have observed different types of oscillatory behavior depending on the laser power that was coupled inside the resonator. For very low (asymptotically null) input power, no thermal oscillation is observed at all. However, above a certain threshold, a relatively smooth oscillatory behavior is observed in the optical output port, as displayed in Fig. 3(a). As the coupled power increases, these oscillations morph into a sharper slow–fast waveform, and the period of the oscillations increases, as well [Fig. 3(b)]. Further increase of the in-coupled power leads to even sharper relaxation oscillations, and also an even longer period for the oscillations [up to half a second; see Fig. 3(c)]. Beyond their unusually long period, a noteworthy feature of these relaxation oscillations is their waveform, which is characterized by a very sharp dip (over a millisecond timescale), followed by another one that is about 1000 times longer.

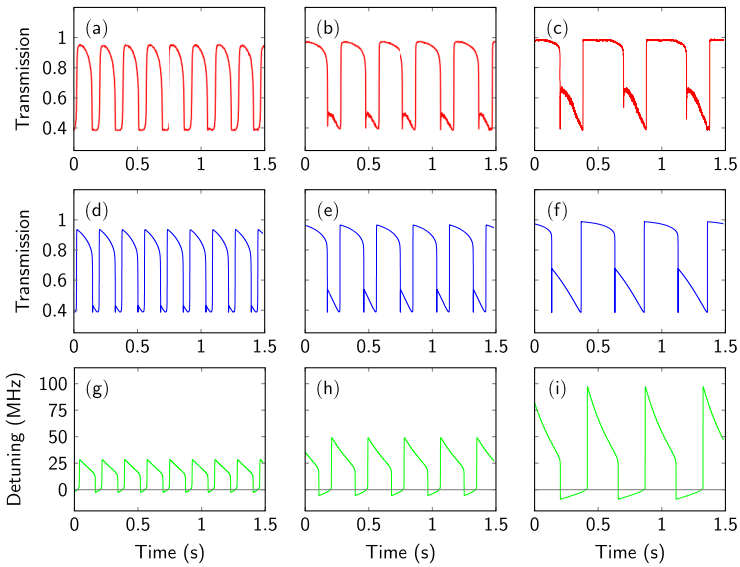

Fig. 3. (a)–(c) Experimental and (d)–(f) numerical time traces of the relaxation oscillations. The numerical variations of the corresponding frequency detunings $\Delta\omega_{\text{th}}(t)/2\pi$ are displayed in (g)–(i). The periods of the relaxation oscillations are (a), (d), and (g) 181 ms; (b), (e), and (h) 290 ms; and (c), (f), and (i) 504 ms. Note that the minima of transmission correspond to zero detunings (light is maximally coupled inside the resonator).

The observed phenomenology at the experimental level is accurately recovered numerically using Eqs. (7) and (8). The physical parameters used for the simulations are $D = 3$ mm, $A_{\text{eff}} = 10^{-11}$ m^2, $n_{\text{eff}} = 1.466$, $n_2 = 2.89 \times 10^{-20}$ W/m^2, $Q = 10^8$, $\omega_L = 1.3 \times 10^{15}$ rad/s, $\gamma_{\text{th1}} = 1.0$ s^{-1}, $\gamma_{\text{th2}} = 10^3$ s^{-1}, $\gamma_{\text{abs1}} = 0.25 \times 10^{-3}$ K/J, and $\gamma_{\text{abs2}} = 1.0$ K/J. For most sets of coupled ordinary differential equations, the fourth-order Runge–Kutta algorithm enables fast and accurate numerical simulations. However, in our case, we are confronted by two practical problems that impede using that well-known algorithm. The first issue is that we have two timescales that are widely split, and the second one is that the largest timescale is exceptionally large. As a consequence, the fourth-order Runge–Kutta algorithm has been found to be so slow that it was impossible to simulate even a single period of the relaxation oscillations. The solution to circumvent this difficulty is to use an adaptive-step-size method such as the Runge–Kutta–Fehlberg algorithm, which is able to reduce significantly the simulation time (down to less than 1 h per relaxation oscillation period in a computer).

The results of the numerical simulation are presented in Figs. 3(d)–3(f). The intracavity power was increased through laser power, and was set to 45, 71, and 200 mW in Figs. 3(d), 3(e), and 3(f), respectively. An excellent agreement between numerical and experimental is achieved, and it is noteworthy that both the characteristic shape of the temporal profile and the period of the relaxation oscillations can be matched almost perfectly. The analysis of the temperature-induced frequency detuning in Figs. 3(g)–3(i) shows that the fast-timescale dynamics essentially originate from the crossing of the zero-detuning state, which corresponds to maximal light absorption and minimal transmission. The sharpest peak is associated to a fast (almost vertical) crossing, while the wide peak is associated with a much slower crossing. The ratio between the fast and slow timescales is essentially defined by the parameters α_i (temperature-to-frequency conversion factors), $\gamma_{\text{th},i}$ (relaxation rates), and $\gamma_{\text{abs},i}$ (absorption capacity of the laser heat). The consistent trend is that, as the in-coupled power increases, the period of the relaxation increases, as well. In particular, such a phenomenology is important for sensing applications, where this period variation can be linked to a change in one of the system's parameters [6]. It is also important to note that a key ingredient for the observation of these relaxation oscillations is the fact that the thermo-refractive and thermo-elastic coefficients are of opposite sign, while thermal locking occurs otherwise.

In conclusion, we have evidenced for the first time, to the best of our knowledge, thermo-optical oscillations in a mm-size ultrahigh-Q WGM resonator pumped by a resonant CW laser. We have demonstrated that the resonance shifts induced by the thermic coefficients and the Kerr nonlinearity trigger giant relaxation oscillations with a second timescale. Our numerical simulations, which are based on a time-domain set of nonlinear differential equations, are in excellent agreement with experimental results. This work is expected to lead to a better understanding of thermal effects on mm-size resonators, which are core components in many photonics systems for sensing, metrology, and coherent microwave/lightwave generation.

Funding. Centre National d'Etudes Spatiales (CNES); European Research Council (ERC); Labex ACTION; Région Franche-Comté.

Acknowledgment. The authors acknowledge logistic support for super-computation at the Mésocentre de Franche-Comté.

REFERENCES

1. A. B. Matsko, A. A. Savchenkov, N. Yu, and L. Maleki, J. Opt. Soc. Am. B **24**, 1324 (2007).
2. A. A. Savchenkov, A. B. Matsko, V. S. Ilchenko, N. Yu, and L. Maleki, J. Opt. Soc. Am. B **24**, 2988 (2007).
3. M. C. Collodo, F. Sedlmeir, B. Sprenger, S. Svitlov, L. J. Wang, and H. G. L. Schwefel, Opt. Express **22**, 19277 (2014).
4. I. Teraoka, Opt. Commun. **310**, 212 (2014).
5. M. Agarwal and I. Teraoka, Appl. Phys. Lett. **101**, 251105 (2012).
6. Y. Deng, F. Liu, Z. C. Leseman, and M. H. Zadeh, Opt. Express **21**, 4653 (2013).
7. F. Sedlmeir, Z. Zeltner, G. Leuchs, and H. G. L. Schwefel, Opt. Express **22**, 30934 (2014).
8. F. Vollmer and S. Arnold, Nat. Methods **5**, 591 (2008).
9. T. Kippenberg, R. Holzwarth, and S. Diddams, Science **332**, 555 (2011).
10. A. E. Fomin, M. L. Gorodetski, I. S. Grudinin, and V. S. Ilchenko, J. Opt. Soc. Am. B **22**, 469 (2006).
11. I. S. Grudinin and K. J. Vahala, Opt. Express **17**, 14088 (2009).
12. L. He, Y. F. Xiao, J. Zhu, S. K. Ozdemir, and L. Yang, Opt. Express **17**, 12 (2009).
13. I. S. Grudinin, H. Lee, T. Chen, and K. Vahala, Opt. Express **19**, 7365 (2011).
14. T. J. Johnson, M. Borselli, and O. Painter, Opt. Express **14**, 817 (2009).
15. V. B. Braginsky, M. L. Gorodetsky, and V. S. Ilchenko, Phys. Lett. A **137**, 393 (1989).
16. G. Lin, S. Diallo, R. Henriet, M. Jacquot, and Y. K. Chembo, Opt. Lett. **39**, 6009 (2014).